Hindawi
Journal of Sensors
Volume 2023, Article ID 9818716, 1 page
https://doi.org/10.1155/2023/9818716

Retraction

Retracted: Design of Active Display Stand Combing the Pressure Sensor and Kinematics Algorithm

Journal of Sensors

Received 19 December 2023; Accepted 19 December 2023; Published 20 December 2023

This article has been retracted by Hindawi following an investigation undertaken by the publisher [1]. This investigation has uncovered evidence of one or more of the following indicators of systematic manipulation of the publication process:

(1) Discrepancies in scope
(2) Discrepancies in the description of the research reported
(3) Discrepancies between the availability of data and the research described
(4) Inappropriate citations
(5) Incoherent, meaningless and/or irrelevant content included in the article
(6) Manipulated or compromised peer review

The presence of these indicators undermines our confidence in the integrity of the article's content and we cannot, therefore, vouch for its reliability. Please note that this notice is intended solely to alert readers that the content of this article is unreliable. We have not investigated whether authors were aware of or involved in the systematic manipulation of the publication process.

Wiley and Hindawi regrets that the usual quality checks did not identify these issues before publication and have since put additional measures in place to safeguard research integrity.

We wish to credit our own Research Integrity and Research Publishing teams and anonymous and named external researchers and research integrity experts for contributing to this investigation.

The corresponding author, as the representative of all authors, has been given the opportunity to register their agreement or disagreement to this retraction. We have kept a record of any response received.

References

[1] M. Ma and L. Yong, "Design of Active Display Stand Combing the Pressure Sensor and Kinematics Algorithm," *Journal of Sensors*, vol. 2022, Article ID 9275062, 8 pages, 2022.

Hindawi
Journal of Sensors
Volume 2022, Article ID 9275062, 8 pages
https://doi.org/10.1155/2022/9275062

Research Article

Design of Active Display Stand Combing the Pressure Sensor and Kinematics Algorithm

Minhai Ma and Lei Yong

College of Mechanical and Electrical Engineering, Ningbo Polytechnic, Ningbo, 315800 Zhejiang, China

Correspondence should be addressed to Minhai Ma; 1001719@nbpt.edu.cn

Received 23 May 2022; Revised 17 June 2022; Accepted 29 June 2022; Published 23 July 2022

Academic Editor: Yuan Li

To solve the trouble of cervical vertebra disease caused by long working hours, this work is aimed at designing an active monitor stand to achieve the best dynamic trajectory planning. The stand operation system consists of image input, face positioning, and robotic arm. According to the user's face positioning, the inverse kinematics method is used to calculate the steering angle in each direction, and the height and angle are adjusted to make the corresponding selection for the user's display position on the screen. The C++ is used to program the algorithm, and its core is to control the rotation speed of the motor to ensure that the display screen will not cause any interference to the normal work of the user when the bracket moves. In the inverse operation, the Piper method is used to solve the inverse kinematics issues. After testing, the sliding wedge stroke of the developed active display stand is 0.6 mm, and the height position difference at the reference zero point after the display stand is measured with a digital altimeter is 7.12 mm, which indicates that the stand shows a large deformation after being mounted. This work is of important reference value for realizing the movement of active display stand.

1. Introduction

In today's development of the information society, computers and the Internet have become a major part of people, especially young and middle-aged people, in their work and life [1–3]. However, "computer disease" caused by improper operation also appears, especially cervical spondylosis. Common symptoms include neck pain, numbness in fingers, and dizziness. If it is due to improper computer use, it can lead to muscle tension and fatigue in the neck, resulting in degeneration of the discs and facet joints in the neck. As a result, the monitor stand came into being [4–6]. Most of modern office and study need to face the computer for a long time. The height and low angle of the monitor are adjusted through the monitor stand. The appropriate monitor position helps to improve the sitting posture of the human body.

At present, most of the display screens on the market are manually adjusted or use a physical method to maintain the height of the screen, and it is impossible to adjust the user's state at any time [7–9]. The lifting frame of the adjustable liquid crystal display (LCD) screen can flexibly adjust the height of the LCD screen and obtain a comfortable experience of using the computer. In the display system of the computer, the trajectory planning, navigation, and obstacle avoidance functions of the robotic arm of the monitor stand play key functions [10, 11]. Kumar et al. [12] performed a kinematic analysis of the motion degrees of freedom of the stent, thereby addressing the total inverse, rotational inverse, and forward kinematics.

This work is mainly aimed at the computer users who have been sitting for a long time, using the principle of pressure sensing and motion, to design a bracket that can control the stepper motor so that the monitor can move slowly and autonomously without affecting people's office, so as to prevent the occurrence of cervical spondylosis. The system consists of image input, face positioning, and robot arm. According to the current face and the center of the camera, the inverse kinematics method is used to calculate the steer-

ing angle in each direction and adjust the height and angle to provide the user with a suitable display position. The use of active display brackets ensures that the display fixed calipers of the rack can realize multiangle rotation adjustment of screen rotation of 360°, lateral rotation of ±180°, and upper arm lateral rotation of 360°, allowing users to have a larger adjustment range and multiple adjustment viewing angles. The stepper motor controlled by the 51 single-chip microcomputer proposed and designed in this work can make the monitor move slowly and autonomously without affecting the office work, so that the office worker can prevent cervical spondylosis unconsciously. In addition, the design cost is low, and the space occupied is relatively small.

2. Materials and Methods

2.1. How the Active Display Stand Works. The main part of the display stand is the boom, "cantilever" as it literally means it can spread freely like an arm. In addition, it is made of aluminum or carbon steel, fixed diagonally, protected on all four sides, and can be rotated without opening the clip. The monitor stand mainly includes the upper support arm, the lower support arm, the monitor connector, and the platen fixing device. The most important core part is located on the upper support arm, which uses the elastic deformation of the upper arm to support the monitor [13–15]. Compared with the original base, the advantages of the active display stand are obvious. It can be retracted and hovered at any height, the screen can be rotated at 360°, and it can maintain a certain field of view. In addition, it does not occupy the desktop space, easy to manage the desktop, and realize the combination of multiple screens at the same time. There are two main types of monitor mounts on the market today: air spring and mechanical. The pneumatic spring type monitor stand has good handling and good handling performance, but its usage time is lower than that of the mechanical type. Due to the long-term action of the air spring, the sealing performance will decrease, resulting in a decrease in the service life. The types of common robotic arm monitor brackets are shown in Table 1.

Figure 1 shows the track on which the display moves. The designed bracket rail is square; and 1, 2, 3, and 4 are the four end points of the rail. The length of the bracket diagonal rail is represented by L1 and L2, and the angle between the diagonal and each side is 45°. The display screen is connected to the guide rail, and the pulley is adopted to move slowly along the track according to the set program. The set program allows the display screen to move only at an angle of 45 degrees [16, 17]. To achieve smooth motion and no noise when the display is moved to the end, the trajectory of the corresponding tips of 1, 2, 3, 4, and diagonal intersection 5 is designed to be smooth, resulting in a 45 degree rotation at the end, and when cornering, torque is minimized. This maintains stability for the maintenance of the motor and even the entire mobile support system. According to the above description, after a cycle of trajectory movement, the good effect of 360° activity of the cervical spine can be achieved without affecting the work of the office worker.

2.2. Single-Chip Pressure Measurement and Control System. Most computer monitor pedestals have no adjustment function during operation. Most of the current display brackets are based on weight and realize multiangle adjustment, but the manufacturing cost is high due to their many structures [18–20]. Due to the inappropriate cooperation between people and devices, there are often many redundant connecting rods, and automatic adjustment of the connecting rods cannot be realized during operation. The C++ is used to program the algorithm, and the core is to control the rotation speed of the motor to ensure that the display screen will not cause any interference to the normal work of the workers during movement. C++ has rich library functions, fast operation speed, high compilation efficiency, and good portability and can directly control the system hardware. By designing a cyclic function, the display is made to perform periodic line movements. The steering of the motor is controlled by the program to achieve the purpose of turning the display at a 45° angle. Then, the speed of the stepper motor is controlled by the delay() function, thereby controlling the movement speed of the display.

The pressure measurement control device mainly monitors the pressure of the support. Each device is equipped with four sensors, which can connect the hydraulic cavity of the support column, balance jack, and probe jack [21–23]. After the receipt of the instruction of the communication measurement and control system, the pressure of the four channels was measured, and then, the four sound pressure signals were transmitted to the measurement and control center through the communication measurement and control system and then transmitted to the ground through the communication measurement and control center. The pressure measurement control system is equipped with a button; when pressed, the pressure value of the four channels can be displayed in the LCD window cyclically. In the pressure measurement control system, 80C51 expands 8K EPROM (27C64) and 8 K SRAM (6264) as external program memory and data memory. The lower 6 MHz is selected as the operating frequency of the 80C51 single-chip microcomputer, which can meet the data acquisition requirements and reduce the power consumption of the single-chip microcomputer. The basic hardware composition controlled by the single-chip microcomputer is shown in Figure 2.

In the display stand control system developed in this work, its communication and each measurement and control system belong to the master-slave communication network. To adapt to this long-distance, multipoint, and large-interference communication condition, the RS-485 interface is selected. The interface using MAX483 is a small transceiver for RS-485 produced by MAXIM, including a driving device and a receiving device. The device is characterized in that the transmission speed of the driving device can be reduced to the maximum, the interference of electromagnetic waves can be reduced to the maximum, and the influence caused by incorrect cable termination can be reduced.

2.3. Robotic Arm Control Based on Pressure Sensor. As the tactile unit of the robotic arm skin, the pressure sensor needs

Table 1: Common robotic arm monitor stand.

Type of robotic arm	Functions and characteristics	Craft and design	Application scenarios
Wall-mounted rocker	Installed and fixed on the wall, the display can be adjusted at large angles, front and rear, left and right	Aluminum alloy casting or carbon fiber composite material, relying on bolt locking device to achieve rotation angle	Libraries, exchanges, and training institutions,
Stand-up rocker arm	Installed and fixed on the desktop, the monitor can be adjusted front and rear, left and right angles	Aluminum alloy casting or carbon fiber composite material, relying on bolt locking device to achieve rotation angle	Office, studio, and meeting room
Taili multiscreen	Multiple monitors can be moved left and right at the same time, and the tilt angle can be adjusted	Aluminum alloy casting or carbon fiber composite material, relying on bolt locking device to achieve rotation angle	Studio, exchange monitoring center, and home intelligent monitoring system

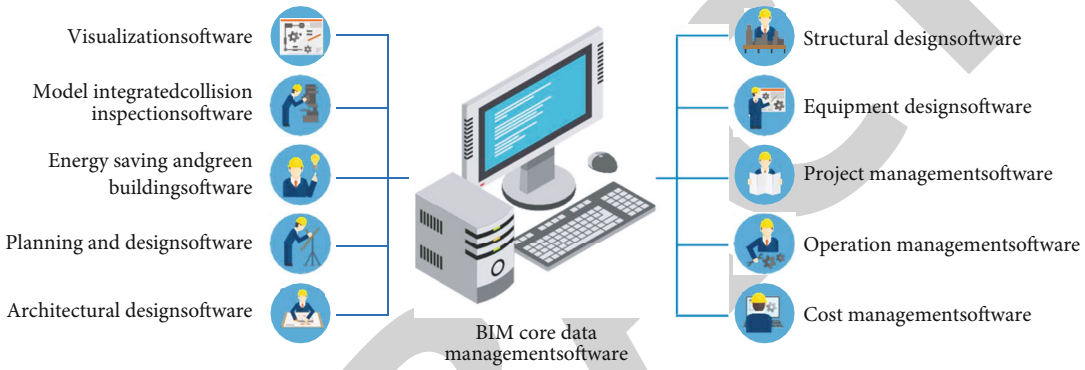

Figure 1: Movement track of the display.

to have two characteristics. Firstly, the overall physical properties of the sensor, such as sensitivity and detection range, meet the design standards; secondly, the sensor must be flexible enough to be attached to the cylindrical surface of the robotic arm [24–26]. The robot's forelimb is equipped with 6 groups of pressure sensors, with a total of 388 detection points, which can conduct a comprehensive detection of the robot's body surface. The two arrays are arranged as a set and are connected to a piece of sensing circuit. When a pressure is applied to the sensor, the circuit converts the voltage value into a pressure value, such as analog multiplexer, signal amplification, and ADC sampling. Among them, the acquisition card of the pressure sensor mainly uses the D/A conversion circuit for analog output [27, 28]. The detectors are arranged horizontally on the testing machine, and then, the detection objects are placed in the corresponding places. Through the detection of the target, the target is detected by the sensor array and processed through the acquisition loop to obtain the corresponding specific value, and then, the table is programmed through the MATLAB program to obtain the stereo image of the detected object. On this basis, a method for detection is presented, as shown in Figure 3.

The pressure-sensitive element MPU6050 developed in this work is based on micro mechanics. The sensor system includes a three-axis accelerometer, a three-axis gyrometer, and an adaptive thermometer. The system can be used for

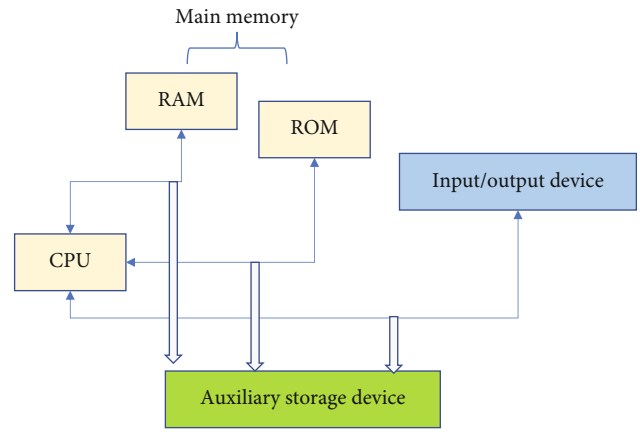

Figure 2: The basic hardware composition of single-chip microcomputer control.

the measurement of various parameters, such as acceleration, velocity, orientation, and displacement. Firstly, the various wires are connected on the robotic arm of the monitor stand to the computer terminal, and then, it is squeezed hard with both hands to measure the working state of the pressure sensor in the human body. The system has high flexibility and elasticity, which not only ensures the safety of the inner

sensor but also ensures the safety in human-machine interaction. The pressure distribution test device developed in this paper has good elasticity and uses a 0.1 mm thick mesh tactile pressure sensor, which enables pressure detection on a variety of contact surfaces.

Tekscan's pressure sensors are two thin polyacetate membranes that are arranged in the shape of a wellhead and arranged in a fence. The outer surfaces of these wires are coated with a special varistor. The pressure between the two contacting surfaces is tested with a flexible membrane sensor. In addition, with dedicated acquisition software and software, the pressure between the gaps can be better understood to optimize product design, quality, and production. Compared with the conventional method, this method not only is cost-effective but also obtains the effect of the test in an intuitive and real-time manner. In this work, the local averaging method is used to predict the measurement results. In the pressure value area, it should select a point as a section, average the pressures of all pressure measuring points in this section, and use this value to replace the pressure of this pressure measuring point:

$$h(i,j) = \frac{1}{M}\sum_{(k,l)\in N} f(k,l)\times\omega_{k,l},$$
$$\sum_{(k,l)}\omega_{k,l} = M. \tag{1}$$

In the above two equations, $f(k,l)$ refers to the pressure value at position (k,l) within the field N, M is the sum of the pressure measurement points within the field, and $\omega_{k,l}$ is the weighting factor.

The data of each collection point of the body pressure distribution sensor is undertaken as a variable, and the pressure value of the collection point in each distribution map as a sample; the pressure distribution histogram can be obtained. $(X_1, X_2 \cdots X_n)$ is set as the pressure value sequence of each collection point; then, the calculation formula of the statistic can be expressed as

$$S^2 = \frac{1}{n-1}\sum_{i=1}^{n}\left(X_i - \bar{X}\right)^2,$$
$$\bar{X} = \frac{1}{n}\sum_{i=1}^{n} X_i. \tag{2}$$

In the above two equations, S^2 represents the variance of the collected pressure value samples.

2.4. Robotic Arm Kinematics Algorithm for the Display Stand. Since the length of the connecting rod of the robotic arm is known, the final position and direction of the end-effector can be determined as long as the rotation angle of each joint are determined, which is called forward kinematics. If the final position and orientation of the end-effector are known, the angle of each joint can also be derived, which is called inverse kinematics. There are two types of inverse kinematics algorithm solutions: one is an analytical solution,

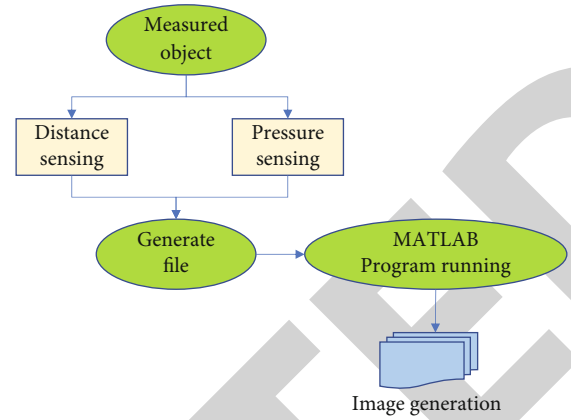

Figure 3: Test flow of sensor acquisition system.

and the other is a numerical solution. MATLAB uses a numerical solution method, which can be understood as iterative optimization, or approximate solution. The positive kinematics solution of the tandem robot is relatively simple, which is just a transformation of position and attitude. This time, the standard D-H algorithm (rotate around the z-axis first) is used to push it to the positive kinematics solution. It can specify a reference coordinate system for each joint axis, determine the relationship between any two adjacent coordinate systems, and obtain the total transformation matrix from the robotic arm end effector to the base coordinate system.

$$T = A_1A_2A_3A_4A_5A_6. \tag{3}$$

In equation (3), T is the transformation matrix of the robot end position, and A_i is the transformation matrix of the i-th axis.

In the inverse kinematics algorithm, since the axes of the three axes of the robot end intersect at one point, which satisfies the piper algorithm, the piper algorithm is used to derive the inverse solution. The robotic arm structure in Figure 4 shows that the axes of the three axes at the end of the robotic arm intersect at the position where axis 5 is located, that is, the wrist point position. From the perspective of the reference coordinate system, if the angles of the first three axes are determined, the position of the wrist point will also be fixed, and the angles of the last three axes only affect the posture of the wrist point, not the position of the wrist point.

In the case of different joint angles of the actuator, the attitude and position expression of the end effector relative to the coordinate system that acts as a reference are different, which is a problem solved by the forward kinematics of the robot. The plane geometry method is adopted to inversely solve the three middle joints, all of which rotate in the vertical plane. The projection of the robotic arm on the xy plane in Figure 5 illustrated that the coordinate (x, y) of the end point P consists of three parts, $(x_1 + x_2 + x_3, x_1 + x_2 + x_3)$. Among it, θ_1, θ_2, and θ_3 are the angles of the steering gear to be solved, and α is the angle between the joint carrying the display and the horizontal plane.

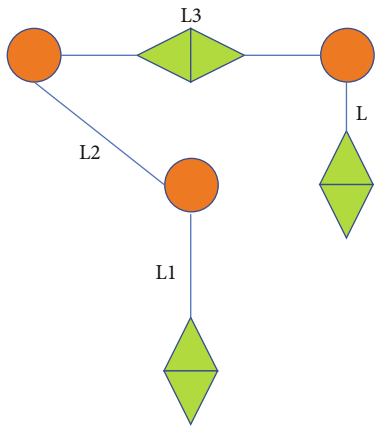

Figure 4: The structure of robotic arm.

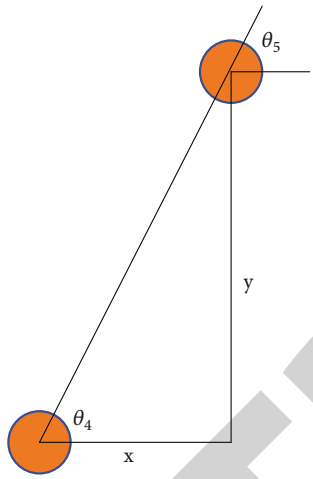

Figure 5: Projection of robotic arm on xy plane.

It should calculate from the base coordinate system the lengths of the connecting rods which are L_1 and L_2, respectively. It should choose a fixed coordinate system $\{0\}$ with the origin coincident with the base joint and assume that the actuator $\{3\}$ is fixed on the second link. The orientation of the actuator coordinate system Cartesian coordinate (x, y) is undertaken as a function of joint angle (θ_1, θ_2); the equation is as follows:

$$\begin{aligned} x &= L_1 \cos\theta_1 + L_2 \cos(\theta_1 + \theta_2) + L_2 \cos(\theta_1 + \theta_2 + \theta_3), \\ y &= L_1 \sin\theta_1 + L_2 \sin(\theta_1 + \theta_2) + L_2 \sin(\theta_1 + \theta_2 + \theta_3), \\ \phi &= \theta_1 + \theta_2 + \theta_3. \end{aligned} \tag{4}$$

The wedge mechanism is an important mechanism to realize power transmission and movement direction conversion, and its mechanism is mainly composed of an active wedge and a driven sliding wedge. Commonly used wedge mechanisms are horizontal motion wedge mechanism and inclined motion wedge mechanism. In the mechanism, under the action of vertical external force, the wedge moves vertically downward, while the sliding wedge moves horizontally to the left or right. On the premise of ignoring the friction of the inclined plane, set the vertical pressure from the wedge to be, and the horizontal resistance of the sliding wedge to be; then the horizontal sliding wedge resistance is as follows:

$$F = \frac{P}{\tan\theta}. \tag{5}$$

The wedge angle is set as θ, and the wedge stroke as L; then the sliding wedge stroke can be expressed as follows:

$$S = L \times \tan\theta. \tag{6}$$

When the three-section wedge mechanism is designed, it is first required that the upper and lower wedges will not fall off horizontally in the wedge groove and ensure that the wedge and sliding wedge have sufficient horizontal sliding wedge stroke and vertical wedge stroke when sliding. This ensures the effective use of the three-section wedge locking structure.

3. Results and Discussion

3.1. Active Safety Control of Display Stand Robotic Arm. Based on the robot kinematics, the desired trajectory of the robotic arm is tracked and controlled by taking the position, velocity, and acceleration of the robotic arm end or each degree of freedom as expectations. When the robotic arm is in contact with the object during the movement, it is the control of restricted motion. This kind of control not only requires the robotic arm to move along a certain trajectory but also controls the contact force between it and the environment. In the robotic arm safety control research experimental platform, a flexible skin with a pressure sensing array can be wrapped on the robotic small arm. By observing the indicator light of the pressure signal acquisition circuit board, the working status of the sensor can be monitored in real time to ensure the stable operation of the sensor. The safe detour experiment consists of two parts: the upper detour and the lower detour. The corresponding joint angle changes are shown in Figures 6 and 7.

When the robotic arm senses that there is an obstacle ahead, it will follow up slowly. When it reaches a certain close distance, the robotic arm suspends its movement and judges the size of the obstacle gap. If it is confirmed that the gap cannot be passed and the new passable area is detected above the robotic arm, the robotic arm performs a small pullback motion and moves upward. When the robotic arm perceives an obstacle ahead, it will follow up slowly. When it reaches a certain close distance, the robotic arm suspends its movement and judges the size of the obstacle gap. If it is confirmed that the gap cannot be passed and the new passable area is detected under the robotic arm, the robotic arm performs a small pullback motion and moves downward.

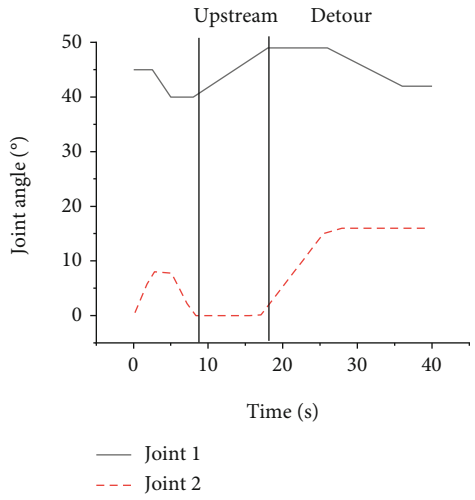

Figure 6: Joint angle change during upper detour.

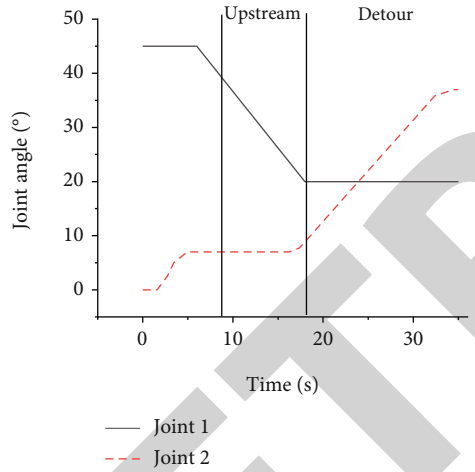

Figure 7: Joint angle change during lower detour.

3.2. Functional Testing of the Display Stand. The rotating arm assembly is installed on the pole assembly, and the height of the arm assembly from the desktop is required to be 230 mm. The active control method is mainly that the robotic arm can foresee the occurrence of danger and adopt safe strategies to avoid danger. A digital altimeter is adopted to measure the height dimension of the bracket before it is mounted, and its height is set as the reference zero point, and the sliding wedge stroke of the bracket is 0.6 mm. Figure 8 is a schematic diagram of the reference zero point of the display stand. A digital altimeter is adopted to measure the height position difference at the reference zero point after the monitor bracket is mounted; it is 7.12 mm, which indicates that there is a large deformation phenomenon after the bracket is mounted. Compared with the maximum displacement deformation of 10.55 mm obtained by the finite element analysis of the arm assembly, the two are approximately equal, indicating that the overall stiffness and strength of the monitor stand meet the technical requirements of the original design.

Figure 8: Schematic diagram of the reference zero point of the monitor stand.

4. Conclusion

At present, LCD has been widely used, and various new display support structures have appeared. In this work, the static display is moved according to the set trajectory. The designed bracket is mainly assembled by the supporting main rod, the positioning and erecting plate, the monitor holder, and the host holding arm and other parts. According to the pressure sensing and the kinematic algorithm of the robotic arm, the three-stage oblique wedge-shaped locking device can be used to easily complete the disassembly and locking of the display stand. The pressure sensor is the tactile element of the robotic arm. It has the comprehensive physical characteristics of the sensor and can touch the human body efficiently and quickly. Secondly, the sensor is elastic and can be attached to the cylindrical surface of the robotic arm. With 51 single-chip microprocessor as the core, the core control system development of active display stand is realized. It is implemented by a loop function to achieve a periodic linear movement. Using the inverse kinematics method, the movement direction of each joystick is calculated, and the precise positioning of the joystick is achieved through the angle and height of the robotic arm. The sliding wedge stroke of the active monitor stand developed in this work is 0.6 mm. The height position difference at the reference zero point is 7.12 mm after the monitor stand is measured with a digital altimeter, indicating that the stand has a large deformation after being mounted.

Due to the complexity of the ROS system, the full-parameter kinematics algorithm of the manipulator cannot

be integrated in ROS, and the follow-up work can consider the forward kinematics of the manipulator. In the following research, since the practical promotion of the active display stand designed in this study should still be a difficult process, it is necessary to continuously update the algorithm iteratively and improve the user experience of the system.

Data Availability

The data used to support the findings of this study are included within the article.

Conflicts of Interest

The authors declare no conflicts of interest regarding the publication of this paper.

Acknowledgments

This work was supported by 2020 Visiting Engineer of Colleges and Universities in Zhejiang Province, Research on Modeling Design of Display Bracket Based on Perceptual Intention (Project No. FG2020042).

References

[1] M. Rana and V. Mittal, "Wearable sensors for real-time kinematics analysis in sports: a review," *IEEE Sensors Journal*, vol. 21, no. 2, pp. 1187–1207, 2020.

[2] W. Pitt, S. H. Chen, and L. S. Chou, "Using IMU-based kinematic markers to monitor dual-task gait balance control recovery in acutely concussed individuals," *Clinical biomechanics*, vol. 80, article 105145, 2020.

[3] J. S. Tan, S. Tippaya, T. Binnie et al., "Predicting knee joint kinematics from wearable sensor data in people with knee osteoarthritis and clinical considerations for future machine learning models," *Sensors*, vol. 22, no. 2, p. 446, 2022.

[4] P. Lisiński, A. Wareńczak, K. Hejdysz et al., "Mobile applications in evaluations of knee joint kinematics: a pilot study," *Sensors*, vol. 19, no. 17, p. 3675, 2019.

[5] L. Pacher, C. Chatellier, R. Vauzelle, and L. Fradet, "Sensor-to-segment calibration methodologies for lower-body kinematic analysis with inertial sensors: a systematic review," *Sensors*, vol. 20, no. 11, p. 3322, 2020.

[6] A. Triantafyllou, G. Papagiannis, S. Stasi et al., "Application of wearable sensors technology for lumbar spine kinematic measurements during daily activities following microdiscectomy due to severe sciatica," *Biology*, vol. 11, no. 3, p. 398, 2022.

[7] H. Chander, E. Stewart, D. Saucier et al., "Closing the wearable gap—part III: use of stretch sensors in detecting ankle joint kinematics during unexpected and expected slip and trip perturbations," *Electronics*, vol. 8, no. 10, p. 1083, 2019.

[8] G. Di Raimondo, B. Vanwanseele, A. van der Have et al., "Inertial sensor-to-segment calibration for accurate 3d joint angle calculation for use in OpenSim," *Sensors*, vol. 22, no. 9, p. 3259, 2022.

[9] J. L. Escalona, P. Urda, and S. Muñoz, "A track geometry measuring system based on multibody kinematics, inertial sensors and computer vision," *Sensors*, vol. 21, no. 3, p. 683, 2021.

[10] Z. A. Abro, Z. Yi-Fan, C. Nan-Liang, H. Cheng-Yu, R. A. Lakho, and H. Halepoto, "A novel flex sensor-based flexible smart garment for monitoring body postures," *Journal of Industrial Textiles*, vol. 49, no. 2, pp. 262–274, 2019.

[11] N. Haralabidis, D. J. Saxby, C. Pizzolato, L. Needham, D. Cazzola, and C. Minahan, "Fusing accelerometry with videography to monitor the effect of fatigue on punching performance in elite boxers," *Sensors*, vol. 20, no. 20, p. 5749, 2020.

[12] S. Kumar, B. Bongardt, M. Simnofske, and F. Kirchner, "Design and kinematic analysis of the novel almost spherical parallel mechanism active ankle," *Journal of Intelligent & Robotic Systems*, vol. 94, no. 2, pp. 303–325, 2019.

[13] H. Keshavarzi, C. Lee, M. Johnson, D. Abbott, W. Ni, and D. L. M. Campbell, "Validation of real-time kinematic (RTK) devices on sheep to detect grazing movement leaders and social networks in merino ewes," *Sensors*, vol. 21, no. 3, p. 924, 2021.

[14] V. Shia, T. Y. Moore, P. Holmes, R. Bajcsy, and R. Vasudevan, "Stability basin estimates fall risk from observed kinematics, demonstrated on the Sit-to-Stand task," *Journal of Biomechanics*, vol. 72, pp. 37–45, 2018.

[15] S. Y. Shin, R. K. Lee, P. Spicer, and J. Sulzer, "Quantifying dosage of physical therapy using lower body kinematics: a longitudinal pilot study on early post-stroke individuals," *Journal of Neuroengineering and Rehabilitation*, vol. 17, no. 1, pp. 1–9, 2020.

[16] B. Oubre, J. F. Daneault, K. Boyer et al., "A simple low-cost wearable sensor for long-term ambulatory monitoring of knee joint kinematics," *IEEE Transactions on Biomedical Engineering*, vol. 67, no. 12, pp. 3483–3490, 2020.

[17] A. Szafarczyk, "Kinematics of mass phenomena on the example of an active landslide monitored using GPS and GBInSAR technology," *Journal of Applied Engineering Science*, vol. 17, no. 2, pp. 107–115, 2019.

[18] R. L. Greene, M. L. Lu, M. S. Barim et al., "Estimating trunk angle kinematics during lifting using a computationally efficient computer vision method," *Human Factors*, vol. 64, no. 3, pp. 482–498, 2022.

[19] S. A. Evans, K. Ballhause, D. A. James, D. Rowlands, and J. B. Lee, "The development and validation of an inertial sensor for measuring cycling kinematics: a preliminary study," *Journal of Science and Cycling*, vol. 10, no. 3, pp. 34–44, 2021.

[20] C. Young, M. L. Oliver, and K. D. Gordon, "Design and validation of a novel 3D-printed wearable device for monitoring knee joint kinematics," *Medical Engineering & Physics*, vol. 94, pp. 1–7, 2021.

[21] B. J. C. Bastiaansen, E. Wilmes, M. S. Brink et al., "An inertial measurement unit based method to estimate hip and knee joint kinematics in team sport athletes on the field," *JoVE (Journal of Visualized Experiments)*, vol. 4, no. 159, article e60857, 2020.

[22] C. Talens-Estarelles, J. J. Esteve-Taboada, V. Sanchis-Jurado, Á. M. Pons, and S. García-Lázaro, "Blinking kinematics characterization during digital displays use," *Graefe's Archive for Clinical and Experimental Ophthalmology*, vol. 260, no. 4, pp. 1183–1193, 2022.

[23] P. Pujayanto, R. Budiharti, E. Adhitama, N. R. A. Nuraini, and H. V. Putri, "The development of a web-based assessment system to identify students' misconception automatically on linear kinematics with a four-tier instrument test," *Physics Education*, vol. 53, no. 4, article 045022, 2018.

[24] M. Affam and P. E. Baffoe, "sing photogrammetric methods for mapping geological structures and predicting pitwall kinematics at the persus mine, Ayanfuri of Ghana," *Ghana Journal of Technology*, vol. 4, no. 2, pp. 66–79, 2020.

[25] V. Groenhuis, A. Nikolaev, S. H. Nies et al., "3-d ultrasound elastography reconstruction using acoustically transparent pressure sensor on robotic arm," *IEEE Transactions on Medical Robotics and Bionics*, vol. 3, no. 1, pp. 265–268, 2020.

[26] H. Lin, J. Tan, J. Zhu et al., "A programmable epidermal microfluidic valving system for wearable biofluid management and contextual biomarker analysis," *Nature Communications*, vol. 11, no. 1, pp. 1–12, 2020.

[27] J. Zhang, J. Chen, M. Li et al., "Design, fabrication, and implementation of an array-type MEMS piezoresistive intelligent pressure sensor system," *Micromachines*, vol. 9, no. 3, p. 104, 2018.

[28] L. Xiang, X. Zeng, F. Xia, W. Jin, Y. Liu, and Y. Hu, "Recent advances in flexible and stretchable sensing systems: from the perspective of system integration," *ACS Nano*, vol. 14, no. 6, pp. 6449–6469, 2020.